Korean J. Chem. Eng., 39(4), 1028-1035 (2022)
DOI: 10.1007/s11814-021-0967-1

pISSN: 0256-1115
eISSN: 1975-7220

Influence of the sorption pressure and K_2CO_3 loading of a MgO-based sorbent for application to the SEWGS process

Do Yeong Ryu[*,,‡], Seongbin Jo[***,‡], Tae-Young Kim[*], Soo Yeong In[*], Jae Kuk Kim[**], Jae Eun Hwang[**], Jae Chang Kim[*,†], and Soo Chool Lee[****,†]**

*Department of Chemical Engineering, Kyungpook National University, Daegu 41566, Korea
**JnK Co., Ltd, Daegu 41566, Korea
***Department of Chemical and Environmental Engineering, University of California-Riverside, Riverside, California 92521, United States
****Research Institute of Advanced Energy Technology, Kyungpook National University, Daegu 41566, Korea
(*Received 4 August 2021 • Revised 27 September 2021 • Accepted 29 September 2021*)

Abstract−MgO-based sorbents were prepared by impregnation with K_2CO_3 at different loadings. This study examined the CO_2 absorption and regeneration properties of MgO-based sorbents at various pressures. The CO_2 capture capacity of the PMI-30 sorbent increased to 204.4 mg CO_2/g sorbent with increasing absorption pressure through CO_2 absorption by MgO itself and K_2CO_3 by generating structures, such as $MgCO_3 \cdot 3H_2O$ and $K_2Mg(CO_3)_2$. However, no $KHCO_3$ phase was observed after CO_2 absorption at 1, 10, and 20 atm. The CO_2 capture capacity of the MgO and PMI-10, 20, 30, and 40 sorbents was the 94.6, 129.9, 156.6, 204.4, and 239.4 mg CO_2/g sorbent, respectively. The CO_2 capture capacity of MgO in the PMI sorbent was relatively constant regardless of the decreasing MgO content and increasing K_2CO_3 content. The CO_2 absorption ability of MgO was calculated by substracting theoretical CO_2 capture capacity of K_2CO_3 from the total capacity of sorbents. The TPD experiment performed at 1 atm after CO_2 absorption at 20 atm showed that the regeneration temperature of the PMI sorbents differed according to the K_2CO_3 loading.

Keywords: CO_2 Capture, Pre-combustion, K_2CO_3, MgO-based Sorbent, $K_2Mg(CO_3)_2$

INTRODUCTION

Carbon dioxide (CO_2) is a significant greenhouse gas released into the atmosphere by the combustion of coal in coal-fired power plants. A CO_2 capture process is necessary at coal-fired power plants to reduce energy loss and global warming. Therefore, many researchers have attempted to develop CO_2 capture technologies for the CO_2 gas emitted from coal-fired power plants.

CO_2 capture processes at coal-fired power plants can be divided into pre-combustion, post-combustion, and oxyfuel technology. In the pre-combustion capture process, CO_2 capture occurs before combustion. The total pressure in the product gas is 20-70 atm, and the CO_2 content in the dry gas is between 15 and 60%. In addition, the separation of CO_2 in this process is significantly easier than CO_2 separation in post-combustion capture because of the high CO_2 partial pressure [1]. An ideal dry CO_2 sorbent is required under the following conditions: (1) high CO_2 capacity and high sorption rate, (2) high selectivity for CO_2 gas, (3) excellent regeneration property, (4) stable CO_2 capacity for multi cycles, and (5) excellent mechanical strength [2,3].

The development of a CO_2 sorbent for the sorption enhanced water gas shift (SEWGS) process is underway using magnesium oxide, hydrotalcite, calcium oxide, and lithium-containing materials. The calcium-based sorbent is an excellent CO_2 sorbent. However, higher CO_2 sorption and regeneration temperatures of 600-800 °C are needed for effective CO_2 sorption and a stable multicycle [4-10,25]. Representative lithium-containing sorbents are lithium zirconate and lithium orthosilicate, which are manufactured by calcination at temperatures above 850 °C using powder mixing and sol-gel methods. Lithium-containing sorbents have high CO_2 capture capacity (28-32 wt%) at lower sorption temperature than calcium-based sorbents. On the other hand, a high regeneration temperature of approximately 700 °C is needed for stable multicycles [11-13].

Calcium-based and lithium-containing sorbents are unsuitable for the SEWGS process because of the slow CO_2 sorption rate and high energy loss by high regeneration temperatures. Magnesium oxide and hydrotalcite are promising materials for the SEWGS process, and many studies have evaluated K_2CO_3-impregnated magnesium oxide and hydrotalcite. Hydrotalcite has a double-layered structure consisting of positively charged metal hydroxide layers and negatively charged interlayers containing anions and water molecules. The hydrotalcite-based sorbent showed thermal stability, a relatively fast CO_2 sorption rate, and low regeneration temperature between 400 °C and 500 °C. However, it has a low CO_2 capture capacity below 1 mmol/g at atmospheric pressure [12,14,15,24,26]. Maroño et al. [16] examined the effects of the steam partial pressure using K_2CO_3-promoted hydrotalcite. They reported that the K_2CO_3-promoted hydrotalcite sorbent increased to 9 mol/kg with

†To whom correspondence should be addressed.
E-mail: kjchang@knu.ac.kr, soochool@knu.ac.kr
‡Do Yeong Ryu and Seongbin Jo contributed equally to this work.

increasing steam partial pressure from 0 bar to 4.5 bar under the conditions of Pco_2=0.34 bar and 300 °C.

The magnesium-based sorbent can absorb CO_2 gas based on the following reactions:

$$MgO_{(s)}+H_2O_{(g)}\rightarrow Mg(OH)_{2(s)} \quad (1)$$

$$Mg(OH)_{2(s)}+CO_{2(g)}\rightarrow MgCO_{3(s)}+H_2O_{(g)} \quad (2)$$

$$MgCO_{3(s)}+H_2O_{(g)}\rightarrow Mg(OH)_{2(s)}+CO_{2(g)} \quad (3)$$

The magnesium-based sorbent was reported to have moderate CO_2 capture capacity at an intermediate temperature of 200 to 400 °C and a lower regeneration energy than calcium oxide and lithium-containing sorbents [12,15,17-21,23]. Siriwardane et al. [17] developed a regenerable magnesium hydroxide-based sorbent with excellent CO_2 capture capacity at 200 °C and a low regeneration temperature of 400 °C. They described the importance of the rehydroxylation process for converting MgO to $Mg(OH)_2$ during the cooling process in water vapor after CO_2 sorption. The rehydroxylation process is essential for retaining the reactivity during the multicycle. The CO_2 capture capacity of the magnesium hydroxide-based sorbent increased due to a thermodynamically favorable (reaction 2: ΔH^0_{298}=−19.657 kJ/mol). Hassanzadeh et al. [18] developed a MgO-based sorbent using sol-gel and dolomite modification methods. The dolomite-modified CO_2 sorbent showed excellent mechanical strength, high reactivity, and good CO_2 capture capacity at 300-450 °C at 20 atm. This MgO-based sorbent could be regenerated easily at 500 °C at 20 atm. They observed improved CO_2 capture capacity with increasing surface area and porosity because of the transient increase in the number of $Mg(OH)_2$ molecules in the presence of steam during CO_2 sorption. Compared to other CO_2 sorbents, magnesium-based sorbents are most suitable for the SEWGS process in the coal-fired power plant. This MgO-based sorbent has a lower regeneration temperature than the calcium oxide and lithium-containing sorbent. Furthermore, it has good thermal stability and high CO_2 capture capacity than hydrotalcite-based sorbents.

This article reports the effect of CO_2 sorption pressure and K_2CO_3 loading using MgO-based sorbents prepared by the impregnation method. In addition, X-ray diffraction (XRD), thermogravimetric analysis/differential thermal gravimetry (TGA/DTG), and temperature-programmed desorption (TPD) experiments were conducted to examine the CO_2 sorption mechanism, physical changes, and regeneration properties of MgO-based sorbents after CO_2 sorption.

EXPERIMENTAL

1. Preparation of the CO_2 Sorbent

The MgO-based CO_2 sorbents were prepared by the impregnation method using potassium carbonate. Magnesium oxide (Aldrich) was added to an aqueous solution of potassium carbonate (Aldrich) in de-ionized water. The solutions were mixed with a magnetic stirrer at room temperature for 24 hours. After stirring, the mixture was dried in a rotary vacuum evaporator at 60 °C. The dried samples were calcined in a furnace in air for five hours at 500 °C. The calcination temperature was increased to 500 °C at 5 °C/min. The particle size of the MgO-based CO_2 sorbents was 150-250 μm. These CO_2 sorbents are denoted as PMI-*x*, where P, M, I, and *x* are potassium carbonate, magnesium oxide, impregnation method, and the loading amount of potassium carbonate. The MgO sorbent was prepared by physical mixing with magnesium oxide powder

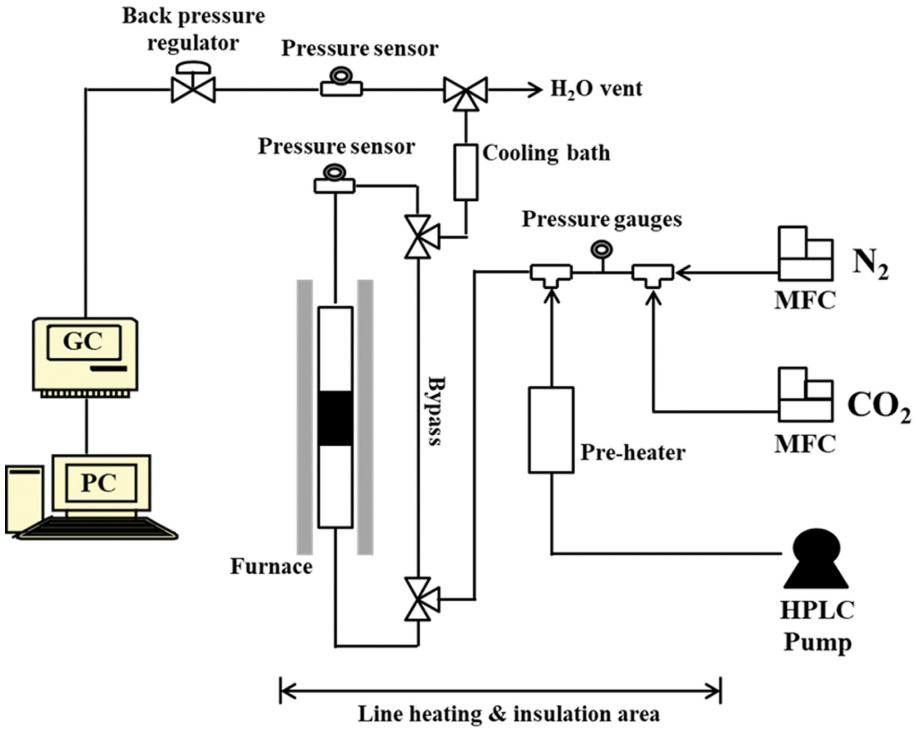

Fig. 1. Schematic diagram of the high-pressure apparatus.

and a small amount of distilled water. The MgO sorbent was calcined in air for five hours at 500 °C. The particle size of MgO sorbent was 150-250 μm.

2. Physical Characteristic Analysis

The changes in the crystalline phase before/after CO_2 sorption were examined by XRD (Philips X'PERT) using Cu Kα radiation at the Korea Basic Science Institute. TGA and DTG (SDT Q600, TA Instrument) were conducted to investigate the thermal characteristics after CO_2 sorption. Nitrogen gas was used as the carrier gas, the CO_2 sorbents were heated to 50 °C to 500 °C at a ramping rate of 5 °C/min. The N_2 adsorption-desorption isotherms at −196 °C were measured using the ASAP 2020 instrument (Micromeritics) to evaluate textural properties such as the Brunauer-Emmett-Teller surface area, pore-volume, and pore size. TPD experiments were conducted at 1 and 20 atm to investigate the regeneration properties of the CO_2 sorbents. The TPD experiment was conducted in a nitrogen atmosphere. The sample was heated from 200 °C to 550 °C at a heating rate of 1 °C/min.

3. Apparatus and Procedures

Fig. 1 shows a schematic diagram of the high-pressure experimental apparatus. The CO_2 capture capacity of the CO_2 sorbents was determined using a fix-bed reactor of stainless steel with an outside diameter of 1 inch. The CO_2 sorbent was dried to remove the moisture and impurities on the sorbent surface under a nitrogen atmosphere for 12 h at 350 °C before packing in the reactor. The CO_2 capture capacity of the CO_2 sorbent was examined by packing 10 g of the sorbent into a stainless steel reactor. The gas hourly space velocity was maintained at 530 h^{-1}. The CO_2 sorption pressure was maintained at 1, 10, and 20 atm using a back pressure regulator. The CO_2 sorption pressure during CO_2 sorption was confirmed using an analog pressure gauge and two digital pressure gauges. The gas flow rates were 10 vol% CO_2, 10 vol% H_2O, and N_2 balance, which were controlled using a mass flow controller. The GC column used in the analysis was a 1/8 inch stainless tube packed with Porapak Q. The outlet gas from the reactor was analyzed automatically every one or two minutes using a thermal conductivity detector equipped with an autosampler (Valco). The CO_2 capture capacity was calculated from the CO_2 breakthrough curve, which indicates the CO_2 absorbed amount until the output concentration of CO_2 reached 10 vol%, which is the same as that of the inlet.

RESULTS AND DISCUSSION

1. CO_2 Capture Capacity According to Pressure

Fig. 2 presents the breakthrough curves (a) and CO_2 capture capacities (b) of MgO and PMI-30 sorbents in the presence of 10 vol% CO_2, 10 vol% H_2O, and a N_2 balance at 200 °C at 1, 10, and 20 atm. In Fig. 2(a), the net breakthrough time of the MgO sorbent was not observed despite the increase in CO_2 sorption pressure. However, the net breakthrough time of the PMI-30 sorbent increased to 0, 6, and 14 min with increasing sorption pressure, showing a seven-fold increase compared to the breakthrough time at 1 atm. The CO_2 capture capacity of the MgO and PMI-30 sorbents was calculated from the CO_2 breakthrough curves of Fig. 2(a), as shown in Fig. 2(b). The CO_2 capture capacity of the MgO sorbent at 1, 10, and 20 atm was the 2.5, 34.2, and 94.6 mg CO_2/g

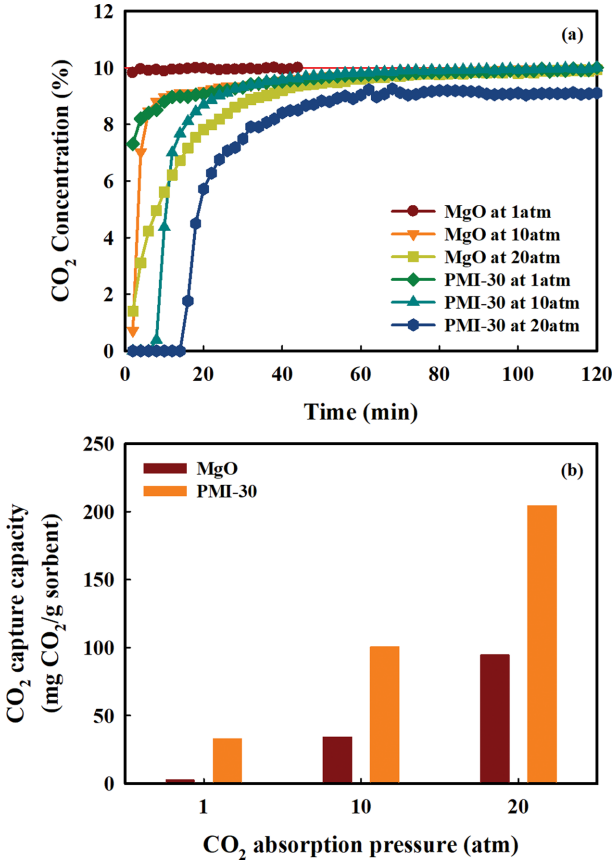

Fig. 2. CO_2 breakthrough curves and CO_2 capture capacity of the MgO and PMI-30 sorbents according to the CO_2 sorption pressure.

sorbent, respectively. At 20 atm, the CO_2 capture capacity of the MgO sorbent had a relatively high CO_2 capture capacity of 94.6 mg CO_2/g sorbent. The CO_2 capture capacity of PMI-30 sorbent at 1, 10, and 20 atm was the 32.8, 100.5, and 204.4 mg CO_2/g sorbent, respectively. In particular, the PMI-30 sorbent at 20 atm showed an excellent CO_2 capture capacity of 204.4 mg CO_2/g sorbent, which is a higher CO_2 sorption capacity than the theoretical value of K_2CO_3 involved within the PMI-30 sorbent. From experimental results of the MgO and PMI-30 sorbents, the MgO sorbent showed a CO_2 capture capacity of 94.6 mg CO_2/g sorbent at 200 °C and 20 atm. The high capture capacity of PMI-30 sorbent was attributed to CO_2 absorption by MgO itself as well as K_2CO_3 in the presence of water vapor at 200 °C and 20 atm [22].

2. X-ray Diffraction after CO_2 Sorption

XRD of the MgO and PMI-30 sorbents was conducted to examine the characteristics before and after CO_2 sorption according to the CO_2 sorption pressure, as shown in Fig. 3. The XRD patterns of PMI-30 sorbent before CO_2 sorption showed only two phases: K_2CO_3 (JCPDS No. 49-1093) and MgO (JCPDS No. 43-1022). In the case of the MgO sorbent, the XRD patterns were similar before and after CO_2 sorption. The XRD patterns of the PMI-30 sorbent after CO_2 sorption at 1 atm showed three phases: K_2CO_3, MgO, and $K_2Mg(CO_3)_2$ (JCPDS No. 75-1725) phase. After CO_2 sorption at 10 and 20 atm, XRD showed four phases, K_2CO_3, MgO,

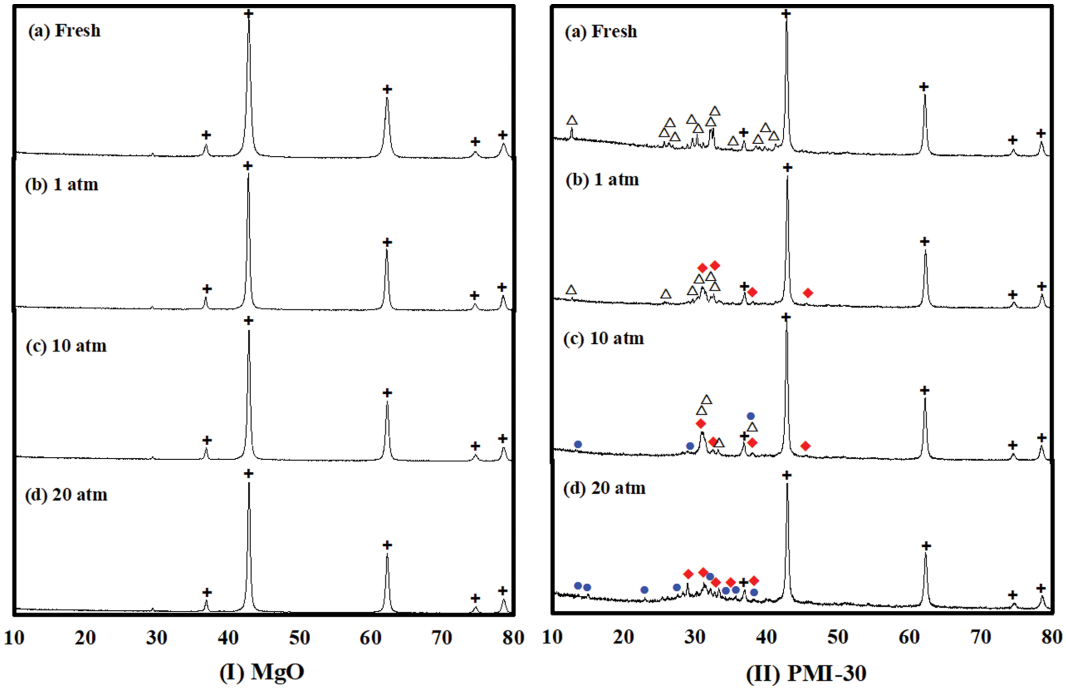

Fig. 3. XRD patterns before/after CO_2 sorption of MgO and PMI-30 sorbents according to the CO_2 sorption pressure; (+) MgO, (△) K_2CO_3, (●) $MgCO_3 \cdot 3H_2O$, (◆) $K_2Mg(CO_3)_2$.

$K_2Mg(CO_3)_2$, and $MgCO_3 \cdot 3H_2O$ (JCPDS No. 01-0130). XRD of PMI-30 sorbent showed no $KHCO_3$ phase after CO_2 sorption regardless of the sorption pressure. Lee et al. [22] examined the CO_2 absorption property of K_2CO_3-impregnated MgO-based sorbents in the presence of water vapor at 60 °C and 1 atm. After CO_2 absorption, XRD revealed new structures such as $K_2Mg(CO_3)_2$ and $K_2Mg(CO_3)_2 \cdot 4(H_2O)$ phases, but no $KHCO_3$ phase was observed after CO_2 absorption at low temperature despite the presence of water vapor. Xiao et al. [20] reported a $K_2Mg(CO_3)_2$ phase in the XRD pattern after CO_2 absorption by the MgO-based sorbents. They described that the $KHCO_3$ phase was not observed after CO_2 absorption at high temperature. XRD confirmed that PMI-30 sorbent after CO_2 sorption at 20 atm consisted of two phases: $K_2Mg(CO_3)_2$ and $MgCO_3 \cdot 3H_2O$. Therefore, PMI-30 sorbent at 20 atm had excellent CO_2 capture capacity due to CO_2 sorption of K_2CO_3 and MgO or CO_2 sorption of MgO itself within the PMI-30 sorbent. However, the MgO sorbent did not show structure changes after CO_2 sorption in the presence of water vapor at 200 °C and 1, 10, and 20 atm.

3. TGA/DTG after CO_2 Sorption

TGA/DTG of MgO and PMI-30 sorbents were conducted to investigate the thermal property after CO_2 sorption. Both MgO and PMI-30 sorbents showed weight loss at temperatures from 30 °C to 100 °C due to the desorption of adsorbed water on the sorbent surface (Fig. 4). The weight loss of MgO sorbent after CO_2 sorption at 1, 10, and 20 atm was 0.00%, 4.45%, and 11.30% at temperatures from 200 °C to 400 °C, respectively. The weight loss from the MgO sorbent was more than that of the CO_2 capture capacity at 10 and 20 atm. The DTG peaks of MgO sorbent showed one peak at the same temperature range as the weight loss range of TGA. MgO sorbent did not show structural changes after CO_2 sorption regardless of the CO_2 sorption pressure, as shown in Fig. 3(I). TGA/DTG confirmed that the MgO sorbent showed higher weight loss than the CO_2 capture capacity at 10 and 20 atm. The higher weight loss than the CO_2 capture capacity suggests that $MgCO_3$ and $Mg(OH)_2$ were generated during CO_2 sorption in the presence of water vapor at 200 °C and 10 and 20 atm [17]. The weight loss of the PMI-30 sorbent was 4.24%, 10.46%, and 20.76% at 1, 10, and 20 atm, respectively, from 200 °C to 400 °C. Those weight losses agreed with the CO_2 capture capacity of PMI-30 sorbent according to the CO_2 sorption pressure shown in Fig. 2. The DTG peak of the PMI-30 sorbent at 1 atm showed one peak between 300 °C and 380 °C due to decomposition of the $K_2Mg(CO_3)_2$ structure. The DTG peaks of the PMI-30 sorbent at 10 and 20 atm showed two peaks between 200 °C to 400 °C due to the decomposition of $MgCO_3$ and $K_2Mg(CO_3)_2$, as confirmed by the XRD patterns in Fig. 3. No $KHCO_3$ structure was found in the PMI-30 sorbent between 100 °C to 200 °C after CO_2 sorption in the presence of water vapor at 1, 10, and 20 atm [22].

4. TPD at 1 and 20 atm of MgO and PMI-30 Sorbents

TPD experiments of MgO and PMI-30 sorbents were conducted to identify the regenerable temperature under 1 and 20 atm and a nitrogen atmosphere from 200 °C to 550 °C. Fig. 5 presents the TPD results. The TPD results of the MgO sorbent at 1 and 20 atm showed one peak at 326 °C due to $MgCO_3$ decomposition, which was generated during CO_2 sorption. The MgO sorbent was regenerable at approximately 370 °C through TPD experiments of 1 and 20 atm. The TPD result of PMI-30 sorbent at 1 atm revealed two peaks at 388 °C and 418 °C due to $MgCO_3$ and $K_2Mg(CO_3)_2$ decomposition, which were generated during CO_2 sorption at 20 atm

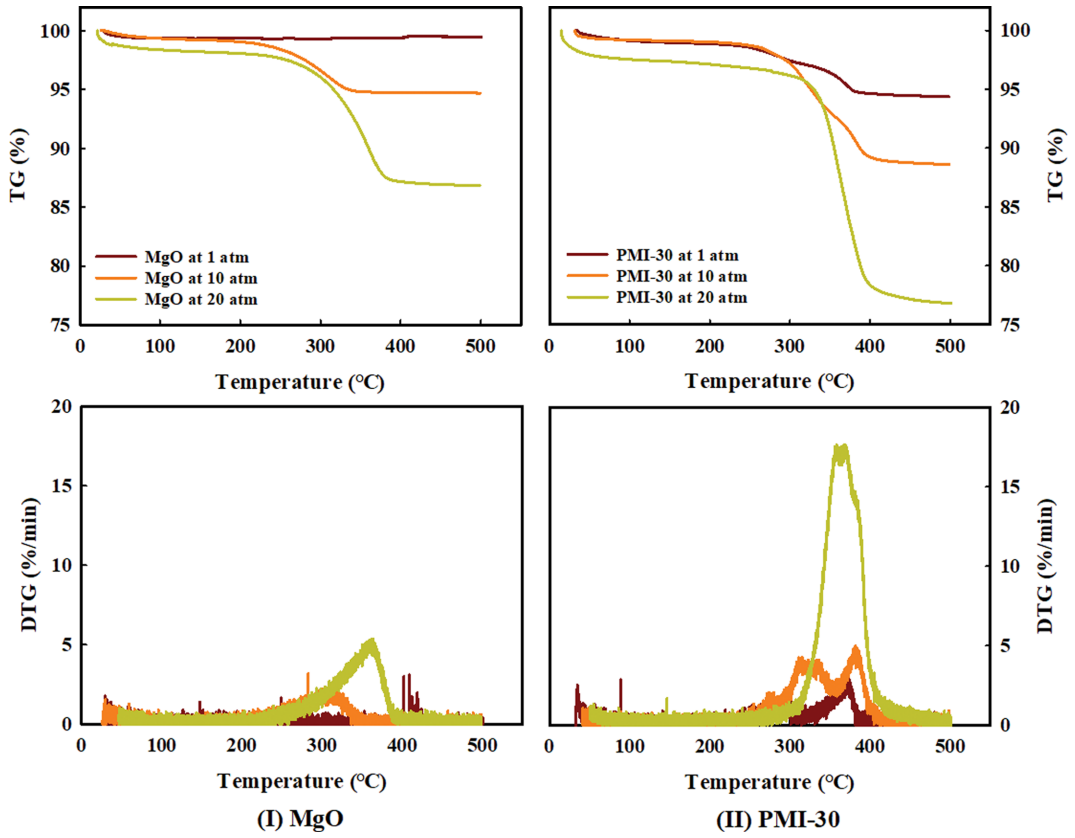

Fig. 4. TGA/DTG curves of MgO and PMI-30 sorbents after CO_2 sorption according to the CO_2 sorption pressure.

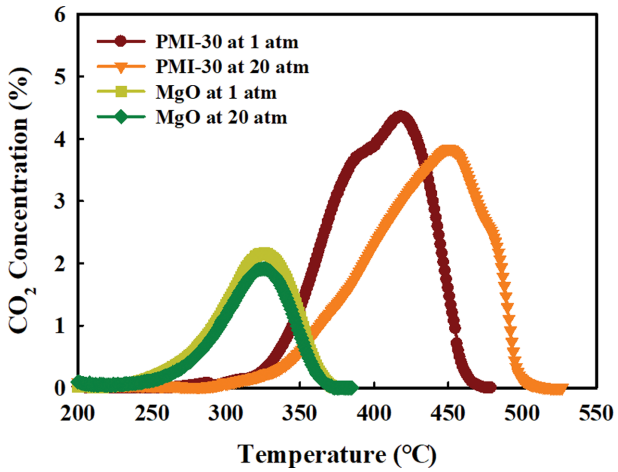

Fig. 5. TPD results of 1 and 20 atm for MgO and PMI-30 sorbents after CO_2 sorption at 20 atm.

[22]. However, the TPD result of PMI-30 sorbent at 20 atm showed a single peak that was different from that obtained at 1 atm. MgO sorbent showed the same regeneration temperature despite the increase in TPD pressure. However, the PMI-30 sorbent confirmed the different regeneration temperatures under TPD conditions of 1 and 20 atm. The shift in the regenerable temperature in an increasing direction was attributed to the different decomposition temperatures of the product, such as $MgCO_3$ and $K_2Mg(CO_3)_2$, by the effect of the regeneration pressure.

Table 1. Textural properties of magnesium and potassium-based magnesium sorbents

Sample name	Surface area (m^2/g)	Pore-volume (cm^3/g)	Pore size (nm)
MgO	38.02	0.31	29.32
PMI-10	34.15	0.29	29.97
PMI-20	23.57	0.23	33.60
PMI-30	22.22	0.21	33.42
PMI-40	16.37	0.15	33.40

5. CO_2 Capture Capacity According to the K_2CO_3 Loading

Table 1 provides information on the surface area, pore-volume, and pore size of MgO and PMI sorbents. The MgO sorbent has a surface area of 38.02 m^2/g, a pore volume of 0.33 cm^3/g, and pore size of 34.61 nm. The surface area and pore-volume of PMI sorbents decrease with increasing K_2CO_3 loading. When the K_2CO_3 loading is 40 wt% (PMI-40 sorbent), the surface area is reduced to about 52% compared to the PMI-10 sorbent, and the pore volume is also significantly reduced. The decrease in surface area and pore-volume is caused by filling the pores with K_2CO_3 or blocking the pore opening with K_2CO_3. The CO_2 capture capacity of the PMI sorbents according to the K_2CO_3 loading was conducted in the presence of 10 vol% CO_2 and 10 vol% H_2O, and a N_2 balance at 200 °C and 20 atm, as shown in Fig. 6. Fig. 6(a) presents the (A) theoretical CO_2 capture capacity of K_2CO_3 and (B) the total CO_2

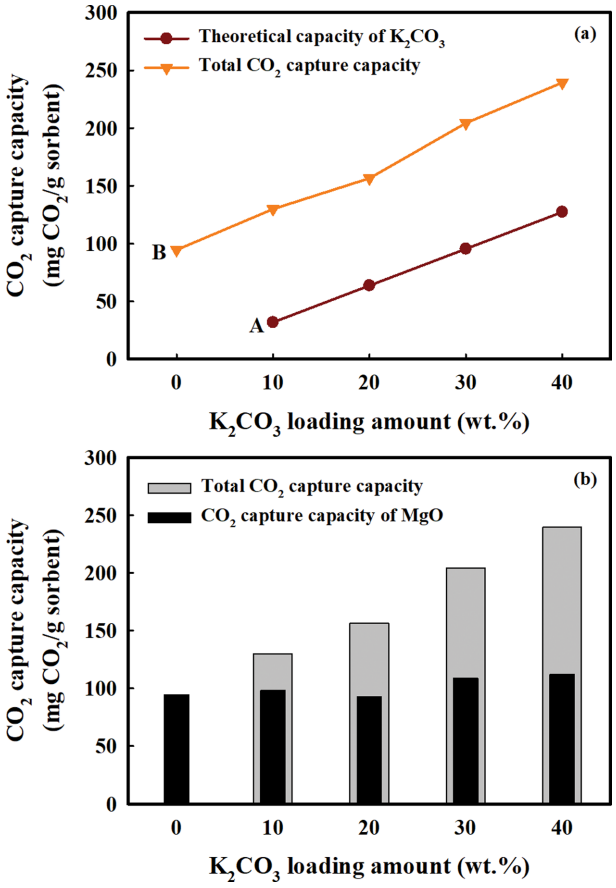

Fig. 6. CO_2 capture capacity of PMI-10 to 40 sorbents according to K_2CO_3 loading at 20 atm.

capture capacity. The experimental CO_2 capture capacity of MgO and PMI-10 to 40 sorbents was 94.6, 129.9, 156.6, 204.4, and 239.4 mg CO_2/g sorbent, respectively, which increased with increasing K_2CO_3 loading. The PMI-10 to 40 sorbents showed higher CO_2 capture capacity than the theoretical CO_2 capture capacity of K_2CO_3 due to the CO_2 sorption of MgO itself. Fig. 6(b) shows the CO_2 capture capacity of MgO within each sorbent according to the K_2CO_3 loading, and it was calculated by substracting theoretical CO_2 capture capacity of K_2CO_3 from total CO_2 capture capacity of sorbents (B-A) in Fig. 6(a). The CO_2 capture capacity of MgO in PMI-*x* sorbent was approximately 94.60, 98.06, 92.92, 108.89, and 112.05 mg CO_2/g sorbent (Fig. 6(b)). The CO_2 capture capacity of the calculated MgO from the PMI sorbents was similar to MgO sorbent despite the decreasing amount of MgO support with increasing K_2CO_3 loading.

Fig. 7 shows the amount of CO_2 sorption per 1 g K_2CO_3 (left: dark red Y-axis) and MgO (right : dark green) as a function of the K_2CO_3 loading. The amount of CO_2 sorption per 1 g K_2CO_3 and MgO was calculated from the CO_2 capture capacity of PMI-10 to 40 sorbents, as shown in Fig. 6. The CO_2 capture capacity of the K_2CO_3 within PMI-10 to 40 sorbents was 318.4 mg CO_2/g K_2CO_3 corresponding theoretical value, respectively. However, the CO_2 capture capacity of MgO within the PMI-10 to 40 sorbents was approximately 109.55, 116.15, 155.56, and 186.75 mg CO_2/g MgO,

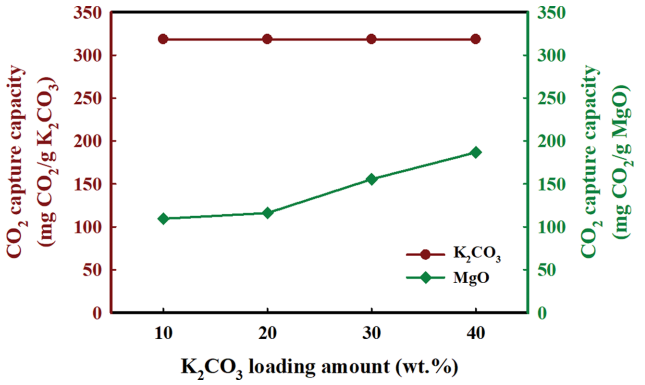

Fig. 7. Amount of CO_2 sorption per 1 g of K_2CO_3 (left: black Y-axis) and MgO (right: dark green) of the PMI-10 to 40 sorbents as a function of the amount of K_2CO_3 and MgO loaded in the presence of 10 vol% CO_2 and 10 vol% H_2O at 200 °C and 20 atm.

respectively. The amount of CO_2 sorption per 1 g MgO increased despite the decreasing amount of MgO support, meaning improvement of CO_2 capture efficiency by MgO.

6. X-ray Diffraction and TPD Results According to K_2CO_3 Loading

XRD analysis of PMI-10~40 sorbents was conducted to identify the structural changes after CO_2 sorption according to the K_2CO_3 loading, as shown in Fig. 8. The XRD patterns of PMI-10 to 40 sorbents before CO_2 sorption showed only two phases: K_2CO_3 and MgO phase (Fig. 8(I)). The peak intensity of K_2CO_3 increased with increasing K_2CO_3 loading. The XRD patterns of PMI-10 and 20 sorbents after CO_2 sorption at 20 atm showed two phases: $K_2Mg(CO_3)_2$ and MgO. The PMI-30 and 40 sorbents after CO_2 sorption at 20 atm showed three phases: $K_2Mg(CO_3)_2$, $MgCO_3{\cdot}3H_2O$, and MgO (Fig. 8(II)). No $MgCO_3{\cdot}3H_2O$ phase was observed in the XRD patterns of the PMI-10 and 20 sorbents regardless of the K_2CO_3 loading and despite having a higher level of MgO support than the PMI-30 and 40 sorbents. However, the PMI-30 and 40 sorbents showed both $K_2Mg(CO_3)_2$ and $MgCO_3{\cdot}3H_2O$ phases with increasing CO_2 capture capacity.

TPD experiments at 1 atm of the PMI-10 to 40 sorbents after CO_2 absorption at 20 atm were conducted to examine the regeneration properties, as shown in Fig. 9. The CO_2 desorption of PMI-*x* sorbents started at 300 °C, and the desorbed CO_2 peak was observed at temperatures ranging from 300 °C to 500 °C. The TPD result of PMI-10 sorbent showed one peak at 376 °C, and the TPD results of PMI-20 to 40 sorbents showed two peaks between 376 and 436 °C. In the case of PMI-10 sorbent, it was a CO_2 peak by the decomposition of $MgCO_3$ than the CO_2 peak by the decomposition of $K_2Mg(CO_3)_2$ due to the low K_2CO_3 loading. In the case of the PMI-20 to 40 sorbents, the CO_2 peak by the decomposition of $K_2Mg(CO_3)_2$ increased due to the increase in the K_2CO_3 loading. Furthermore, the regenerable temperature shifted to a higher temperature with increasing K_2CO_3 loading. The regeneration temperature could be shifted by the amount of CO_2 absorption and bonding strength of the product according to the amount of active material.

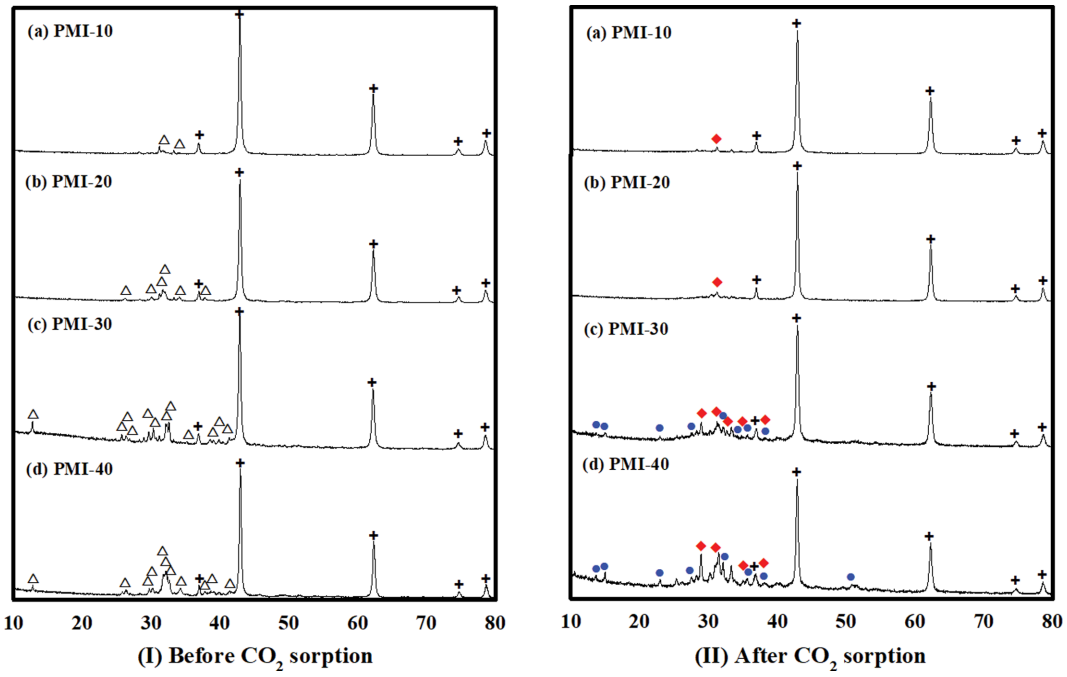

Fig. 8. XRD patterns before/after CO_2 sorption of PMI-10 to 40 sorbents according to the K_2CO_3 loading; (+) MgO, (△) K_2CO_3, (●) $MgCO_3 \cdot 3H_2O$, (◆) $K_2Mg(CO_3)_2$.

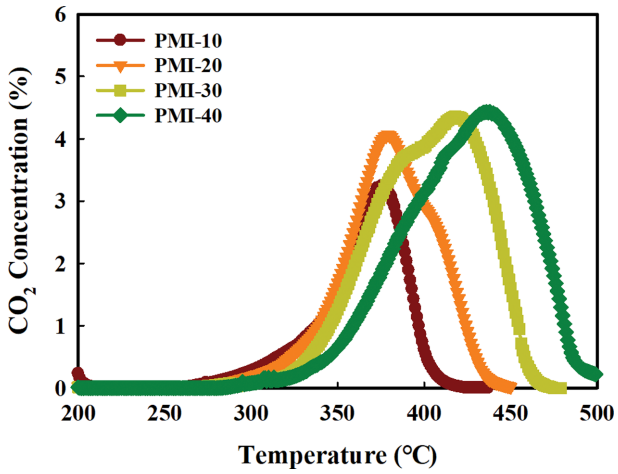

Fig. 9. TPD results at 1 atm of PMI-10 to 40 sorbents after CO_2 sorption at 20 atm according to the K_2CO_3 loading.

CONCLUSION

This study examined the CO_2 absorption and regeneration properties of MgO-based sorbents loaded with K_2CO_3 according to the pressure. The MgO-based sorbent loaded with K_2CO_3, such as PMI-10 to 40, showed excellent CO_2 capture capacity. The excellent CO_2 capture capacity was attributed to the reaction with MgO and K_2CO_3 in the presence of water vapor at 20 atm. The PMI sorbents showed high absorption capacity due to the formation of structures, such as $MgCO_3 \cdot H_2O$ and $K_2Mg(CO_3)_2$, according to XRD. In the case of the regeneration property through TPD, the MgO sorbent showed one peak at 1 and 20 atm, but the regeneration temperature of the PMI-30 sorbent shifted to a higher temperature. The regeneration temperature of the sorbents, according to the K_2CO_3 loading, shifted to a higher temperature at 1 atm. The regeneration temperature increased with increasing amount of active material, such as K_2CO_3.

ACKNOWLEDGEMENT

This work was supported by the Technology Innovation Program (No. 20015460) funded By the Ministry of Trade, Industry & Energy (MOTIE, Korea). This research was supported by National R&D Program through the National Research Foundation of Korea (NRF) funded by Ministry of Science and ICT (No. 2021M3I3 A1084502).

REFERENCES

1. R. Notz, I. Tönnies, N. McCann, G. Scheffknecht and H. Hasse, *Chem. Eng. Technol.*, **34**, 163 (2011).
2. S. C. Lee, Y. M. Kwon, S. Y. Jung, J. B. Lee, C. K. Ryu, C. K. Yi and J. C. Kim, *Fuel*, **104**, 882 (2013).
3. Z. Yong, V. Mata and A. E. Rodrigues, *Sep. Purif. Technol.*, **26**, 195 (2002).
4. H. Lu, E. P. Reddy and P. G. Smirniotis, *Ind. Eng. Chem. Res.*, **45**, 39449 (2006).
5. S. F. Wu, Q. H. Li, J. N. Kim and K. B. Yi, *Ind. Eng. Chem. Res.*, **47**, 180 (2008).
6. L. Li, D. L. King, Z. Nie, X. S. Li and C. Howard, *Energy Fuels*, **24**, 3698 (2010).
7. R. Koirala, K. R. Gunugunri, S. E. Pratsinis and P. G. Smirniotis, *J. Phys. Chem. C*, **115**, 24804 (2011).

8. J. Mastin, A. Arada and J. Meyer, *Energy Procedia*, **4**, 1184 (2011).
9. Z. Zhou, Y. Qi, M. Xie, Z. Cheng and W. Yuan, *Chem. Eng. Sci.*, **74**, 172 (1996).
10. J. M. Valverde, *J. Mater. Chem. A*, **1**, 447 (2013).
11. G. Pannocchia, M. Puccini, M. Seggiani and S. Vitolo, *Ind. Eng. Chem. Res.*, **46**, 6696 (2007).
12. S. H. Choi, J. H. Drese and C. W. Jones, *ChemSusChem.*, **2**, 796 (2009).
13. L. Guo, X. Wang, C. Zhong and L. Li, *Appl. Surf. Sci.*, **257**, 8106 (2011).
14. J. M. Lee, Y. J. Min, K. B. Lee, S. G. Jeon, J. G. Na and H. J. Ryu, *Langmuir*, **26**, 18788 (2010).
15. Q. Wang, J. Luo, Z. Zhong and A. Borgna, *Energy Environ. Sci.*, **4**, 42 (2011).
16. M. Maroño, Y. Torreiro and L. Gutierrez, *Int. J. Greenhouse Gas Control*, **14**, 183 (2013).
17. R. V. Siriwardane and R. W. Steven Jr., *Ind. Eng. Chem. Res.*, **48**, 2135 (2009).
18. A. Hassanzadeh and J. Abbasian, *Fuel*, **89**, 1287 (2010).
19. P. C. Lin, C. W. Huang, C. T. Hsiao and H. Teng, *Environ. Sci. Technol.*, **42**, 2748 (2008).
20. G. Xiao, R. Singh, A. Chaffee and P. Webley, *Int. J. Greenhouse Gas Control*, **5**, 634 (2011).
21. J. C. Fisher II, R. V. Siriwardane and R. W. Steven Jr., *Ind. Eng. Chem. Res.*, **51**, 5273 (2012).
22. S. C. Lee, H. J. Chae, S. J. Lee, B. Y. Choi, C. K. Yi, J. B. Lee, C. K. Ryu and J. C. Kim, *Environ. Sci. Technol.*, **42**, 2736 (2008).
23. C. Zhao, X. Chen, C. Zhao, Y. Wu and W. Dong, *Energy Fuels*, **26**, 3062 (2012).
24. S. Walspurger, L. Boels, P. D. Cobden, G. D. Elzinga, W. G. Haije and R. W. Brink, *ChemSusChem.*, **1**, 643 (2008).
25. S. Liu, J. Ma, L. Guan, J. Li, W. Wei and Y. Sun, *Micropor. Mesopor. Mater.*, **117**, 466 (2009).
26. Z. Liu and W. H. Green, *Ind. Eng. Chem. Res.*, **52**, 9665 (2013).
27. S. D. Kenarsari, M. Fan, G. Jiang, X. Shen, Y. Lin and X. Hu, *Energy Fuels*, **27**, 6938 (2013).